Raman Spectra and Normal Coordinate Analysis of the N1−H and N3−H Tautomers of 4-Methylimidazole: Vibrational Modes of Histidine Tautomer Markers†

Akira Toyama, Kunio Ono,‡ Shinji Hashimoto,§ and Hideo Takeuchi*

Graduate School of Pharmaceutical Sciences, Tohoku University, Aobayama, Sendai 980-8578, Japan

Received: June 26, 2001

The imidazole ring of histidine exists in two tautomeric forms in neutral-to-basic aqueous solution, and the tautomerism of the histidine residue sometimes plays a key role in catalytic reactions of enzymes. We have investigated the molecular vibrations of two tautomers of 4-methylimidazole (4-MeIm), a model compound for the histidine side chain, by Raman spectroscopy and ab initio calculations based on the density functional theory (DFT) approach. Examination of the temperature dependence of Raman intensity revealed nine pairs of bands characteristic of the N1-protonated and the N3-protonated tautomers of 4-MeIm at 1576/1596, 1452/1427, 1304/1344, 1265/1259, 1229/1234, 1165/1149, 1088/1104, 996/1014, and 942/934 cm^{-1}. Five to six pairs of tautomerism-sensitive Raman bands were also identified for each of the C2-, N-, and C2,N-deuterated analogues of 4-MeIm. The observed Raman wavenumbers were used to determine nine scaling factors for the in-plane force constants derived from DFT calculations using the 6-311+G(2d, p) basis set. The force field finally obtained reproduces the experimental vibrational wavenumbers of four additional isotopomers (C5-, C5,N-, C2,C5-, and C2,C5,N-deuterated 4-MeIm) as well. The vibrational modes calculated for 4-MeIm are useful in understanding the origins of the previously proposed tautomer marker bands of histidine at 1568/1585, 1282/1260, 1090/1105, and 983/1004 cm^{-1}. A pair of Raman bands at 1320/1354 cm^{-1} is suggested to be a new tautomer marker of histidine.

Introduction

The imidazole ring of histidine contains two nitrogen atoms (Nπ, Nτ) separated by a carbon atom (C2) in its five-membered ring system. The two nitrogen atoms can be protonated in response to the molecular environment. In aqueous solution at neutral-to-basic pH, one of the nitrogen atoms is protonated and the other is deprotonated, resulting in an electrically neutral ring. The neutral imidazole ring exists as two tautomers that differ from each other in the position of protonation,[1] and the Nτ-protonated (Nτ-H) tautomer is more stable than the Nπ-protonated (Nπ-H) one.[1,2] Since the protonated and deprotonated nitrogens act as a proton donor and an acceptor, respectively, in hydrogen bonding, interactions of a histidine residue with other components of the protein may depend on which tautomer the histidine residue assumes. Furthermore, conversion from one tautomer to the other may facilitate net proton transfer over the imidazole ring. The importance of the histidine protonation and tautomerism in enzymatic reactions has been documented in the literature.[3−5]

Raman spectroscopy provides good probes for the protonation states, including the tautomeric forms, of histidine residues in peptides and proteins.[6−11] Ashikawa and Itoh examined the Raman spectra of histidine and its related compounds under varied temperature and pH conditions.[6] According to their pioneering work, the Nτ-H tautomer of histidine gives three Raman bands at 1568, 1282, and 983 cm^{-1}, while the corresponding Raman bands of the Nπ-H tautomer appear at 1585, 1260, and 1004 cm^{-1}. The three pairs of Raman bands have therefore been regarded as markers of the tautomeric form of histidine. Recently, Noguchi et al. have extended the spectra−tautomer correlation to include the infrared bands at ∼1090 cm^{-1} (Nτ-H) and ∼1105 cm^{-1} (Nπ-H).[12] Although these studies have revealed empirical correlations between the vibrational wavenumbers and tautomeric forms, full understanding of the correlations requires detailed knowledge about the vibrational modes of the imidazole ring.

The normal vibrational modes of the neutral imidazole ring have been studied by ab initio calculations using 4-methylimidazole (4-MeIm, Figure 1) or 4-ethylimidazole as a model compound. Majoube et al. computed the vibrations of the N1-H (Nτ-H in histidine) and N3-H (Nπ-H) tautomers of 4-MeIm at the 6-31G level and compared the theoretical Raman and infrared spectra with experimental ones.[13] Gallouj et al.[14] employed the density functional theory (DFT) method based on the B3LYP formalism[15,16] to compute the vibrational modes of the N1-H form of 4-ethylimidazole with the 6-31G(df, p)-(5d, 7f) basis set. Hasegawa et al. performed a systematic vibrational analysis on four possible protonation forms of 4-MeIm, including the N1-H and N3-H tautomers, by using the B3LYP-DFT method and the 6-31G(df, p) basis set.[17] Although the previous ab initio calculations revealed general features of normal vibrations of the neutral imidazole ring, the computed vibrational wavenumbers were, in some cases, deviated from the experimental ones more than 20 cm^{-1}, a typical wavenumber difference between the two tautomers.

In this study, we have tried to improve the in-plane force field of 4-MeIm by employing a higher approximation in the ab initio calculations and a new strategy in refining the scaling

† Part of the special issue "Mitsuo Tasumi Festschrift".

* Corresponding author. E-mail: takeuchi@mail.cc.tohoku.ac.jp; FAX: +81-22-217-6855.

‡ Present address: Central Research Institute, Ajinomoto Co., Kawasaki 210-0801, Japan.

§ Present address: Science University of Tokyo in Yamaguchi, Onoda 756-0884, Japan.

10.1021/jp0124185 CCC: $22.00
Published on Web 10/02/2001

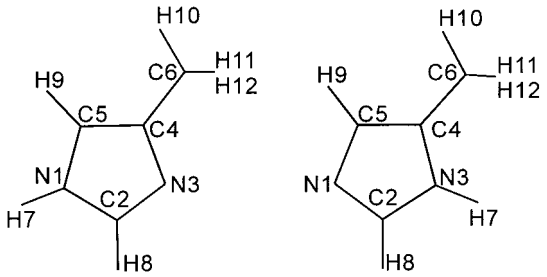

Figure 1. Structures of the N1-H (left) and N3-H (right) tautomers of 4-MeIm.

factors of force constants. To increase the reliability of the force field, the Raman spectral data to be compared with the computational results have been extended to the N1-H and N3-H tautomers of the C2-deuterated analogue in H_2O and D_2O solutions. Since the tautomer-sensitive vibrations are expected to involve atomic motions around the protonated and/or nonprotonated nitrogens, effects of hydrogen bonding have been taken into account in the refinement of the force field. The force field finally obtained reproduces the experimental vibrational wavenumbers of four additional isotopomers (C5-, C5,N-, C2,-C5-, and C2,C5,N-deuterated) of 4-MeIm as well. The vibrational modes calculated for the tautomer marker bands are useful in understanding the origin of the tautomerism sensitivity not only in 4-MeIm but also in histidine.

Methods

Experimental Procedures. 4-MeIm was purchased from Tokyo Kasei Chemicals. Three isotopomers deuterated at C2 (4-MeIm-C2D), C5 (4-MeIm-C5D), or both carbons (4-MeIm-C2D,C5D) were prepared as described previously.[18] Purification of the compounds was performed by decolorization with activated charcoal powder followed by three times recrystallization from water.

Visible Raman spectra of 4-MeIm and 4-MeIm-C2D were excited with 515 nm radiation from an argon ion laser (Coherent Innova 70) and recorded on a Jasco NR-1800 spectrometer equipped with a liquid-nitrogen cooled CCD detector. 4-MeIm and 4-MeIm-C2D were dissolved at a concentration of 1.2 M in H_2O or D_2O, and the pH or pD of the solution was adjusted to 9.8 with NaOH or NaOD. The solution was decolorized with activated charcoal powder and then sealed in a glass capillary tube. The temperature of the sample solution was controlled by mounting the capillary tube on a thermostated copper block. The spectral slit width was 4.5 cm^{-1} and the wavenumber calibration was effected by using the Raman bands of indene. The Raman band of solvent H_2O (1640 cm^{-1}) or D_2O (1204 cm^{-1}) was used as an internal intensity standard. The visible Raman spectra were decomposed into components of the Voigt band shape[19] using a laboratory-made computer program.

UV Raman spectra of 4-MeIm, 4-MeIm-C5D, and 4-MeIm-C2D,C5D in H_2O and D_2O solutions were excited with 240 nm radiation from an H_2−Raman-shifted Nd:YAG laser operating at a 30 Hz repetition rate (Quanta Ray DCR-3G). The UV Raman apparatus was described in a previous paper.[20] The sample powder was dissolved at a concentration of 50 mM in H_2O or D_2O containing 30 mM Na_2SO_4 as an internal Raman intensity standard. The pH (pD) value of the solution was adjusted to ca. 9.0 with NaOH or NaOD. The sample solution was placed in a spinning quartz cell. The spectral slit width was 8 cm^{-1} and wavenumber calibration was made using the Raman bands of cyclohexane-acetonitrile (1:1, v/v).

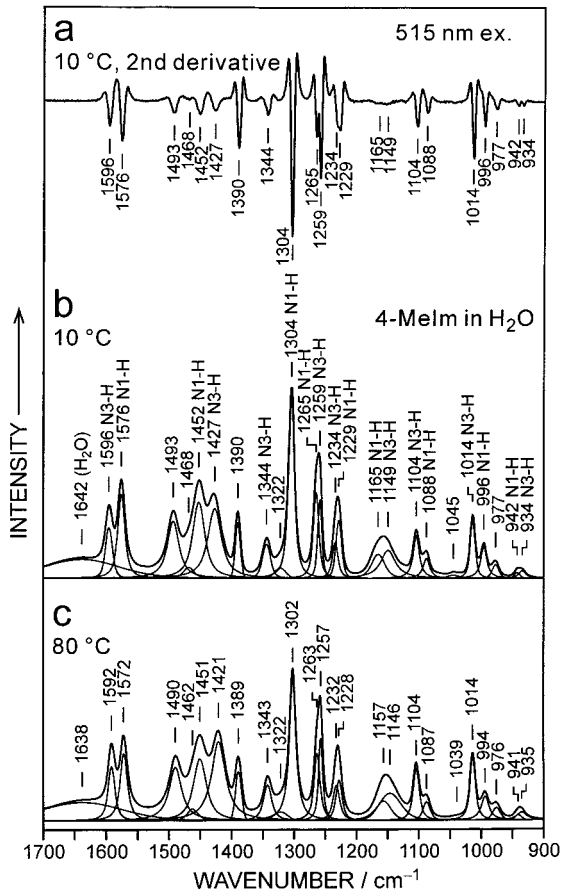

Figure 2. Raman spectra of 4-MeIm in H_2O solution recorded at (b) 10 °C and (c) 80 °C. Trace a shows the second derivative of spectrum b. The sample concentration was about 1.2 M. Thin lines indicate the result of band decomposition with Voigt profiles.

Vibrational Calculations. The DFT calculations were performed using the GAUSSIAN 98 program package[21] with the 6-311+G(2d, p) basis set and the hybrid B3LYP functional approach.[15,16] The force constant matrix obtained was transformed from the Cartesian coordinate system to a nonredundant internal symmetry coordinate system. The internal symmetry force constants were then scaled with nine scaling factors. The vibrational wavenumbers and potential energy distributions were calculated using a modified version of the computer program NCTB.[22,23] Refinements of the scaling factors were made by least-squares fitting of the calculated wavenumbers to the observed ones.

Results and Discussion

Identification of Tautomer Raman Bands. Figure 2 shows the Raman spectrum of 4-MeIm in H_2O solution at 10 °C (b) and 80 °C (c) together with the second derivative curve of the spectrum at 10 °C (a). The second derivative curve clearly indicates the peak positions of 22 sharp Raman bands in the 1700−900 cm^{-1} region, where most Raman bands are expected to arise from in-plane vibrations. In addition to the 22 bands, inspection of the Raman spectrum reveals a broad band at 1642 cm^{-1} due to solvent H_2O and a very weak band at 1045 cm^{-1} ascribable to the out-of-plane rocking mode of the CH_3 group.[13,17,24] Curve fitting of the Raman spectrum with Voigt band profiles suggests the presence of an additional weak band at 1322 cm^{-1}, which may be assigned to the first overtone of a strong Raman band at 660 cm^{-1}.[17] Finally, the Raman spectrum is decomposed into 25 bands as indicated in Figure 2b. In the

TABLE 1: Wavenumbers and Intensities of Raman Bands Observed for 4-MeIm in H_2O at 10 and 80 °C

10 °C		80 °C			
ν^a	I^b	ν^a	I^b	R^c	tautomer
1596	0.27	1592	0.31	1.16	N3-H
1576	0.53	1572	0.44	0.83	N1-H
1493	0.62	1490	0.64	1.02	N1-H + N3-H
1468	0.10	1462	0.10	1.01	N1-H + N3-H
1452	0.83	1451	0.71	0.86	N1-H
1427	0.88	1421	1.04	1.18	N3-H
1390	0.19	1389	0.19	0.98	N1-H + N3-H
1344	0.21	1343	0.25	1.19	N3-H
1322	0.08	1322	0.08	1.00	N1-H + N3-H
1304	0.97	1302	0.87	0.90	N1-H
1265	0.42	1263	0.35	0.85	N1-H
1259	0.27	1257	0.30	1.12	N3-H
1234	0.18	1232	0.21	1.12	N3-H
1229	0.26	1228	0.21	0.81	N1-H
1165	0.26	1157	0.22	0.83	N1-H
1149	0.43	1146	0.47	1.09	N3-H
1104	0.25	1104	0.27	1.08	N3-H
1088	0.13	1087	0.11	0.83	N1-H
1045	0.03	1039	0.01	(0.43)[d]	
1014	0.24	1014	0.30	1.24	N3-H
996	0.19	994	0.17	0.88	N1-H
977	0.07	976	0.07	1.03	N1-H + N3-H
942	0.02	941	0.02	0.86	N1-H
934	0.05	935	0.06	1.18	N3-H

[a] Observed wavenumbers in cm^{-1}. [b] Integrated intensities relative to that of the 1640 cm^{-1} band of solvent water. [c] Intensity ratios I_{80}/I_{10}, where I_{80} and I_{10} stand for the Raman intensities at 80 and 10 °C, respectively. [d] Uncertain because of very weak intensity.

same way, the Raman spectrum recorded at 80 °C is decomposed into 25 bands as shown in Figure 2c. The wavenumbers and integrated intensities of the component bands are summarized in Table 1. Table 1 also shows the intensity ratio $R = I_{80}/I_{10}$ for each band, where I_{80} and I_{10} stand for the Raman intensities at 80 and 10 °C, respectively.

The N1-H tautomer of 4-MeIm is known to be more stable than the N3-H tautomer,[6] and the mole fractions of the N1-H and N3-H tautomers are expected to decrease and increase, respectively, with increase of the temperature. Accordingly, the Raman bands with $R < 1.0$ are assigned to the N1-H tautomer, while those with $R > 1.0$ are ascribed to the N3-H tautomer. Actually, nine Raman bands at 1576, 1452, 1304, 1265, 1229, 1165, 1088, 996, and 942 cm^{-1} have R values less than 0.95 and unequivocally assigned to the N1-H tautomer (Table 1). On the other hand, the bands at 1596, 1427, 1344, 1259, 1234, 1149, 1104, 1014, and 934 cm^{-1} have R values greater than 1.05 and are ascribed to the N3-H tautomer. The other bands with an R value close to 1.0 may be assigned to both tautomers. Of the nine pairs of Raman bands whose wavenumbers are sensitive to the tautomerism, the 1576/1596, 1265/1259, 1088/1104, and 996/1014 cm^{-1} bands may correspond to the previously reported tautomer marker bands of histidine at 1568/1585, 1282/1260, 1090/1105, and 983/1004 cm^{-1}.[6,12] As demonstrated here, examination of the temperature dependence of Raman intensity after spectral decomposition is useful in revealing tautomer Raman bands even if they strongly overlapped each other.

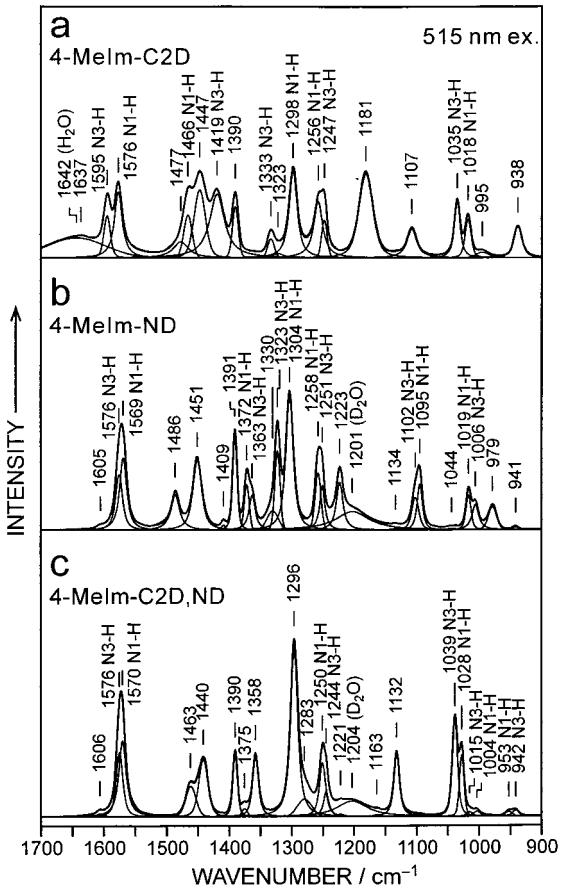

Figure 3. Raman spectra of (a) 4-MeIm-C2D, (b) 4-MeIm-ND, and (c) 4-MeIm-C2D,ND recorded at 5 °C. The sample concentration was about 1.2 M. Thin lines indicate the result of band decomposition with Voigt profiles.

Figure 3 shows the Raman spectrum of 4-MeIm-C2D in H_2O solution (a) together with those of 4-MeIm and 4-MeIm-C2D

TABLE 2: Wavenumbers of Raman Bands Observed for the C2- and N-Deuterated 4-MeIm in Aqueous Solution and the Temperature Dependence of Raman Intensity

4-MeIm-C2D[a]			4-MeIm-ND[b]			4-MeIm-C2D,ND[c]		
ν^d	R^e	tautomer	ν^d	R^e	tautomer	ν^d	R^e	tautomer
1595	1.28	N3-H	1576	1.10	N3-H	1576	1.09	N3-H
1576	0.91	N1-H	1569	0.89	N1-H	1570	0.90	N1-H
1477	0.96	N1-H + N3-H	1486	0.98	N1-H + N3-H	1463	1.01	N1-H + N3-H
1466	0.80	N1-H	1451	1.03	N1-H + N3-H	1440	0.99	N1-H + N3-H
1447	0.96	N1-H + N3-H	1391	0.96	N1-H + N3-H	1390	1.00	N1-H + N3-H
1419	1.18	N3-H	1372	0.93	N1-H	1358	0.98	N1-H + N3-H
1390	0.97	N1-H + N3-H	1363	1.17	N3-H	1296	1.04	N1-H + N3-H
1333	1.20	N3-H	1323	1.16	N3-H	1250	0.84	N1-H
1298	0.92	N1-H	1304	0.91	N1-H	1244	1.22	N3-H
1256	0.91	N1-H	1258	0.89	N1-H	1132	1.02	N1-H + N3-H
1247	1.25	N3-H	1251	1.15	N3-H	1039	1.18	N3-H
1181	1.04	N1-H + N3-H	1223	0.98	N1-H + N3-H	1028	0.91	N1-H
1107	1.00	N1-H + N3-H	1102	1.12	N3-H	1015	1.32	N3-H
1035	1.22	N3-H	1095	0.92	N1-H	1004	0.93	N1-H
1018	0.88	N1-H	1019	0.93	N1-H	953	0.91	N1-H
995	0.99	N1-H + N3-H	1006	1.21	N3-H	942	1.26	N3-H
938	1.01	N1-H + N3-H	979	1.01	N1-H + N3-H			
			941	1.03	N1-H + N3-H			

[a] 4-MeIm-C2D in H_2O solution. [b] 4-MeIm in D_2O solution. [c] 4-MeIm-C2D in D_2O solution. [d] Wavenumbers (cm^{-1}) observed at 5 °C. [e] Intensity ratios I_{60}/I_5, where I_{60} and I_5 stand for the integrated intensities at 60 and 5 °C, respectively.

TABLE 3: Geometrical Parameters Optimized for the N1-H and N3-H Tautomers of 4-MeIm

bond lengths (Å)			bond angles (deg)		
	N1−H	N3−H		N1−H	N3−H
N1C2	1.3612	1.3085	N1C2N3	111.48	111.40
C2N3	1.3107	1.3669	C2N3C4	106.10	107.69
N3C4	1.3805	1.3819	N3C4C5	109.64	104.36
C4C5	1.3698	1.3697	C4C5N1	105.74	111.16
C5N1	1.3806	1.3777	C5N1C2	107.05	105.39
C4C6	1.4927	1.4901	N3C4C6	121.57	123.23
N1H7	1.0065		C2N1H7	126.55	
N3H7		1.0072	N1C2H8	122.53	126.15
C2H8	1.0790	1.0790	C2N3H7		126.23
C5H9	1.0767	1.0789	N1C5H9	122.14	121.47
C6H10	1.0913	1.0901	C4C6H10	111.13	109.64
C6H11	1.0929	1.0945	C4C6H11	110.85	112.03

TABLE 4: Internal Symmetry Coordinates for the In-plane Vibrations of 4-MeIm

			stretch		
S1	νN1H {νN3H}[a]	S2	νC2H	S3	νC5H
S4	νC4C6	S5	νC5N1	S6	νC4C5
S7	νN3C4	S8	νC2N3	S9	νN1C2
S10	CH_3 symmetric stretch (ν_sCH_3)[c]				
S11	CH_3 degenerate stretch (ν_dCH_3)[c]				
			bend		
S12	δN1H {δN3H}[a]	S13	δC2H	S14	δC5H
S15	δC4C6				
S16	$0.2\,\phi$(C5N1C2) − $0.5\,\phi$(N1C2N3) + $0.6\,\phi$(C2N3C4) − $0.5\,\phi$(N3C4C5) + $0.2\,\phi$(C4C5N1)[b] {$0.6\,\phi$(C5N1C2) − $0.5\,\phi$(N1C2N3) + $0.2\,\phi$(C2N3C4) + $0.2\,\phi$(N3C4C5) − $0.5\,\phi$(C4C5N1)}[a,b] (δring1)[c]				
S17	$-0.6\,\phi$(C5N1C2) + $0.4\,\phi$(N1C2N3) − $0.4\,\phi$(N3C4C5) + $0.6\,\phi$(C4C5N1)[b] {$0.4\,\phi$(N1C2N3) − $0.6\,\phi$(C2N3C4) + $0.6\,\phi$(N3C4C5) − $0.4\,\phi$(C4C5N1)}[a,b] (δring2)[c]				
S18	CH_3 symmetric deformation (δ_sCH_3)[c]				
S19	CH_3 degenerate deformation (δ_dCH_3)[c]				
S20	CH_3 rock (ρCH_3)[c]				

[a] The coordinates in braces are for the N3−H tautomer. [b] ϕ represents bending. [c] Abbreviations of the coordinates are given in parentheses.

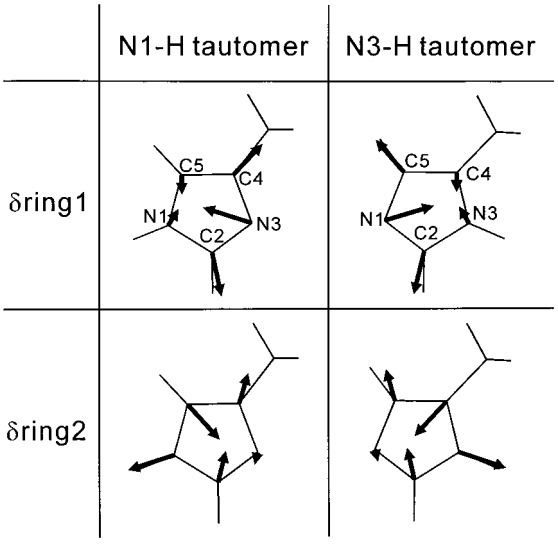

Figure 4. Definitions of two ring deformation coordinates of the neutral imidazole ring.

in D_2O solution (b, 4-MeIm-ND; c, 4-MeIm-C2D,ND) at 5 °C. The deuteration at C2 causes extensive spectral changes below 1500 cm^{-1} (compare Figures 2b and 3a), indicating that many in-plane vibrations of the imidazole ring involve atomic motions around C2, and the Raman spectral data of the C2D isotopomer are very useful in refining the force field of 4-MeIm. On the other hand, significant effects of N-deuteration are seen only in the wavenumber regions around 1450 and 1150 cm^{-1} (Figures 2b and 3b). The present vibrational analysis using the data of both C2- and N-deuterated isotopomers are thus expected to provide a significant improvement of the force field compared to the previous vibrational analyses using only the data of N-deuterated isotopomers.[13,17]

TABLE 5: Scaling Factors for the Diagonal Force Constants of 4-MeIm

factor	internal symmetry coordinate[a]	value	error[b]
f_1	νN_pH (νN1H, νN3H)[c], νC2H, νC5H, νC4C5, νC5N1, νN3C4, νC4C6, ν_sCH_3, ν_dCH_3	0.9728	0.0037
f_2	νN_pC2 (νN1C2, νC2N3)[c]	1.0978	0.0127
f_3	νN_nC2 (νC2N3, νN1C2)[c]	0.9212	0.0080
f_4	νC5H, δC4C6, δ_sCH_3, δ_dCH_3	0.9508	0.0028
f_5	δN_pH (δN1H, δN3H)[c]	1.0367	0.0171
f_6	δC2H	1.0077	0.0125
f_7	δring1	0.9370	0.0133
f_8	δring2	1.0187	0.0099
f_9	ρCH_3	1.0078	0.0093

[a] N_p and N_n stand for the protonated and nonprotonated nitrogen atoms, respectively. The off-diagonal force constants were scaled with the geometrical means of the scaling factors for the diagonal force constants. [b] Standard errors of the scaling factors. [c] The coordinates in parentheses are those of the N1−H (first) and N3−H (second) tautomers.

The Raman spectra of 4-MeIm-C2D, 4-MeIm-ND, and 4-MeIm-C2D,ND were also recorded at 60 °C. Table 2 summarizes the wavenumbers, temperature dependences of Raman intensity ($R = I_{60}/I_5$), and assignments to tautomers for individual Raman bands. Not included in the table are very weak Raman bands at 1637 and 1323 cm^{-1} of the C2D isotopomer, those at 1605, 1409, 1330, 1134, and 1044 cm^{-1} of the ND isotopomer, and those at 1606, 1283, 1221, and 1163 cm^{-1} of the C2D,ND isotopomer because they may be assigned to overtones, combinations, and out-of-plane vibrations. The wavenumbers of in-plane fundamentals listed in Tables 1 and 2 were used in the following normal coordinate analysis.

Optimized Structures of the Tautomers. The geometrical parameters optimized for the N1-H and N3-H tautomers of 4-MeIm are listed in Table 3, and the structures are illustrated in Figure 1. It is noted that all bond lengths are slightly shorter than those of the previous DFT calculations,[14,17] possibly reflecting the improvement of the basis set. The largest difference in bond length between the N1-H and N3-H tautomers is seen for the N1−C2 and C2−N3 bonds. If we denote the protonated nitrogen as N_p and nonprotonated one as N_n, the N_p−C2 bond is longer than the N_n−C2 bond by about 0.05 Å. In conjunction with the bond length difference, the N_p−C═C angle is larger than the N_n−C═C angle by 4−7°. The other bond lengths and angles are not much affected by the tautomerization.

Vibrational Force Field. The DFT force constants calculated for the Cartesian coordinates were transformed into those for a set of nonredundant internal symmetry coordinates, which were defined as described by Majoube et al.[13] Exceptions were two ring deformation coordinates, δring1 and δring2 (Table 4). In the original definitions of δring1 and δring2 by Majoube et al.,[13] both protonated and nonprotonated nitrogens (N_p and N_n) are treated equally. In the neutral imidazole ring, however, either N1 or N3 is protonated and the geometry around N_p is significantly different from that at N_n. Furthermore, effects of hydrogen bonding on the force field may also differ between the N_p (proton donor) and N_n (proton acceptor) sites. To take into account the asymmetry, we defined δring1 as a coordinate primarily involving the C2−N_n−C bending and δring2 as another coordinate orthogonal to δring1. The two ring deformation coordinates are illustrated in Figure 4. It is seen that the δring2 has a significant contribution from the C2−N_p−C

TABLE 6: In-plane Vibrations of 4-MeIm

N1-H tautomer			N3-H tautomer		
ν_{obs} [a]	ν_{calc} [b]	assignment (PED)[c]	ν_{obs} [a]	ν_{calc} [b]	assignment (PED)[c]
	3609	νN1H (100+)		3598	νN3H (100+)
	3217	νC5H (99+)		3196	νC2H (87+), νC5H (13+)
	3195	νC2H (99−)		3190	νC5H (87+), νC2H (13−)
	3058	ν_dCH$_3$ (100+)		3066	ν_dCH$_3$ (92+)
	2988	ν_sCH$_3$ (99+)		2974	ν_sCH$_3$ (93+)
1576	1577	νC4C5 (54+), νC4C6 (14−), δC5H (10+)	1596	1598	νC4C5 (43−), δN3H (20+), νC4C6 (15+)
1493	1496	δC2H (35−), νC2N3 (32+), νC5N1 (9−)	1493	1491	δC2H (27+), δ_dCH$_3$ (24+), νN1C2 (23+)
1468	1482	δN1H (37−), νN1C2 (37+), δ_dCH$_3$ (11+)	1468	1463	δ_dCH$_3$ (39−), νC2N3 (28−), δC2H (13+)
1452	1455	δ_dCH$_3$ (73−), νN1C2 (9+)	1427	1431	δN3H (24−), δ_dCH$_3$ (24+), νC4C5 (23−)
1390	1385	δ_sCH$_3$ (98+)	1390	1389	δ_sCH$_3$ (95+)
1304	1308	νC2N3 (46+), νN3C4 (30−), δring2 (15−)	1344	1344	νN1C2 (35+), νN3C4 (28+), δring2 (11−)
1265	1269	νN3C4 (26−), νC4C6 (15+), δC2H (14−)	1259	1263	δC5H (47+), δC2H (26+), νN1C2 (6−)
1229	1228	δC5H (42+), δC2H (26+), νC5N1 (18−)	1234	1232	νC5N1 (31−), νN1C2 (15+), νC4C6 (14+)
1165	1159	νN1C2 (47−), δN1H (28−), δC2H (10+)	1149	1137	νC2N3 (36+), δN3H (28−), δC2H (13+)
1088	1074	νC5N1 (44−), δC5H (20−), δN1H (8+)	1104	1114	νC5N1 (45+), δC5H (16+), δring2 (7+)
996	1001	ρCH$_3$ (53+), νC4C5 (18−), δring2 (12+)	1014	1013	ρCH$_3$ (33+), δring2 (20−), νC4C5 (18−)
977	964	νN3C4 (37+), δring2 (21−), ρCH$_3$ (11+)	977	980	ρCH$_3$ (35−), δring2 (28−), νN3C4 (23−)
942	942	δring1 (54+), δring2 (27−)	934	937	δring1 (69+), νN3C4 (10+)
	653	νC4C6 (42+), δring1 (26+), δring2 (13+)		646	νC4C6 (41+), δring2 (31−), νN3C4 (6+)
	334	δC4C6 (93−), ρCH$_3$ (13−)		321	δC4C6 (93−), ρCH$_3$ (12−)

[a] Wavenumbers (cm^{-1}) observed at 10 °C. Taken from Table 1. [b] Calculated wavenumbers in cm^{-1}. [c] Potential energy distribution (%) followed by the relative vibrational phase.

TABLE 7: In-plane Vibrations of 4-MeIm-C2D

N1−H tautomer			N3−H tautomer		
ν_{obs} [a]	ν_{calc} [b]	assignment (PED)[c]	ν_{obs} [a]	ν_{calc} [b]	assignment (PED)[c]
	3609	νN1H (100+)		3598	νN3H (100+)
	3217	νC5H (100+)		3191	νC5H (100+)
	3058	ν_dCH$_3$ (100+)		3066	ν_dCH$_3$ (92+)
	2988	ν_sCH$_3$ (99+)		2974	ν_sCH$_3$ (93+)
	2372	νC2D (97+)		2372	νC2D (97+)
1576	1576	νC4C5 (56+), νC4C6 (15−), δC5H (11+)	1595	1594	νC4C5 (46−), δN3H (18+), νC4C6 (16+)
1477	1475	δN1H (35−), νN1C2 (32+), δ_dCH$_3$ (20+)	1477	1474	δ_dCH$_3$ (68+), ρCH$_3$ (13+), νN3C4 (8−)
1466	1464	δ_dCH$_3$ (43+), δN1H (14+), νC5N1 (11+)	1447	1444	νC2N3 (48−), νN1C2 (30+), δN3H (17−)
1447	1437	νC2N3 (47−), δ_dCH$_3$ (24−), νN1C2 (22+)	1419	1410	νN1C2 (25+), νC4C5 (22+), δ_dCH$_3$ (19−)
1390	1384	δ_sCH$_3$ (98+)	1390	1389	δ_sCH$_3$ (94+)
1298	1297	νN3C4 (42−), νC2N3 (31+), δring2 (16−)	1333	1332	νN3C4 (27−), νN1C2 (26−), νC5N1 (12+)
1256	1253	νC5N1 (31−), νC4C6 (20+), δC5H (20+)	1247	1245	δC5H (52−), νC5N1 (19+), νC2N3 (16+)
1181	1175	νN1C2 (40−), δN1H (19−), δC5H (13−)	1181	1181	νC5N1 (35+), δN3H (19+), νC2N3 (15−)
1107	1091	νC5N1 (35+), δC5H (29+), δN1H (14−)	1107	1107	νC5N1 (33+), δC5H (15+), νC2N3 (13+)
1018	1017	δring2 (27+), νN3C4 (14−), δring1 (10+)	1035	1027	δring2 (28−), νN3C4 (16−), νC4C5 (8−)
995	995	ρCH$_3$ (56−), νN3C4 (19−), νC4C5 (9+)	995	1001	ρCH$_3$ (63−), νN3C4 (11−), νC4C5 (9+)
938	932	δring1 (48+), δring2 (34−)	938	948	δring1 (59−), δring2 (20+), δC2D (7+)
	857	δC2D (63−), νN3C4 (9−)		852	δC2D (59+), δring1 (16+), νN3C4 (9+)
	651	νC4C6 (41+), δring1 (27+), δring2 (12+)		645	νC4C6 (41+), δring2 (32−), νN3C4 (6+)
	331	δC4C6 (93−), ρCH$_3$ (13−)		318	δC4C6 (93−), ρCH$_3$ (11−)

[a] Wavenumbers (cm^{-1}) observed at 5 °C. Taken from Table 2. [b] Calculated wavenumbers in cm^{-1}. [c] Potential energy distribution (%) followed by the relative vibrational phase.

TABLE 8: In-plane Vibrations of 4-MeIm-ND

N1-D tautomer			N3-D tautomer		
ν_{obs} [a]	ν_{calc} [b]	assignment (PED)[c]	ν_{obs} [a]	ν_{calc} [b]	assignment (PED)[c]
	3217	νC5H (99+)		3196	νC2H (87+), νC5H (13+)
	3195	νC2H (99+)		3190	νC5H (87+), νC2H (13−)
	3058	ν_dCH$_3$ (100+)		3066	ν_dCH$_3$ (92+)
	2988	ν_sCH$_3$ (99+)		2974	ν_sCH$_3$ (93+)
	2652	νN1D (98+)		2643	νN3D (99+)
1569	1568	νC4C5 (60−), νC4C6 (18+), δC5H (11−)	1576	1573	νC4C5 (57−), νC4C6 (18+), δC5H (11−)
1486	1489	δC2H (36+), νC2N3 (33−), νN1C2 (20+)	1486	1487	δC2H (28+), νN1C2 (26+), δ_dCH$_3$ (24+)
1451	1455	δ_dCH$_3$ (77+), νC2N3 (10+)	1451	1454	δ_dCH$_3$ (58−), νN1C2 (15+), δC2H (14+)
1391	1397	νN1C2 (45+), δN1D (18−), νC5N1 (18−)	1391	1391	δ_sCH$_3$ (98+)
1372	1383	δ_sCH$_3$ (88+)	1363	1369	νN3C4 (37+), νC2N3 (35−), δring1 (19−)
1304	1306	νC2N3 (41−), νN3C4 (35+), δring2 (17+)	1323	1337	νN1C2 (40−), νC5N1 (12+), δring2 (12+)
1258	1265	νN3C4 (20+), δC2H (20+), νC4C6 (14−)	1251	1255	δC5H (55+), δC2H (27+), νC5N1 (8−)
1223	1224	δC5H (46−), δC2H (26−), νC5N1 (15+)	1223	1228	νC5N1 (25−), δC2H (19−), νN1C2 (13+)
1095	1098	νC5N1 (23+), νN1C2 (22+), δC5H (11+)	1102	1118	νC5N1 (55−), δC5H (13−), δring2 (6−)
1019	1009	ρCH$_3$ (35+), νC4C5 (20−), δC5H (15+)	1006	1011	ρCH$_3$ (48+), νC4C5 (17−), δring2 (9−)
979	972	νN3C4 (33+), ρCH$_3$ (26+), δring1 (24−)	979	977	δring2 (34+), νN3C4 (14+), ρCH$_3$ (12+)
941	939	δring2 (54+), δring1 (13−), νN1C2 (6+)	941	938	δring1 (61−), νN3C4 (14−)
	855	δN1D (66+), δring1 (22+), νC5N1 (7−)		882	δN3D (65−), δring1 (9+), δring2 (7−)
	651	νC4C6 (42+), δring1 (25+), δring2 (14+)		640	νC4C6 (39+), δring2 (31−), νN3C4 (6+)
	331	δC4C6 (93−), ρCH$_3$ (13−)		316	δC4C6 (93−), ρCH$_3$ (11−)

[a] Wavenumbers (cm^{-1}) observed at 5 °C. Taken from Table 2. [b] Calculated wavenumbers in cm^{-1}. [c] Potential energy distribution (%) followed by the relative vibrational phase.

bending. To a good approximation, δring1 and δring2 are regarded as ring distortions at N_n and N_p, respectively.

In ab initio molecular orbital calculations, the calculated wavenumbers or force constants are usually scaled to make a comparison with the experimental wavenumbers. In this study, we have computed DFT force constants for an isolated molecule of 4-MeIm. To reproduce the experimental vibrational wavenumbers observed in aqueous solution, it may be reasonable to use different scaling factors for the force constants that would be affected differently by hydrogen bonding in the aqueous

TABLE 9: In-plane Vibrations of 4-MeIm-C2D,ND

N1-D tautomer			N3-D tautomer		
ν_{obs} [a]	ν_{calc} [b]	assignment (PED)[c]	ν_{obs} [a]	ν_{calc} [b]	assignment (PED)[c]
	3217	νC5H (100+)		3191	νC5H (100+)
	3058	ν_dCH$_3$ (100+)		3066	ν_dCH$_3$ (92+)
	2988	ν_sCH$_3$ (99+)		2974	ν_sCH$_3$ (93+)
	2652	νN1D (98+)		2643	νN3D (98+)
	2371	νC2D (97+)		2371	νC2D (97+)
1570	1568	νC4C5 (60−), νC4C6 (18+), δC5H (11−)	1576	1571	νC4C5 (59−), νC4C6 (19+), δC5H (11−)
1463	1466	δ_dCH$_3$ (66+), ρCH$_3$ (9+), νN1C2 (7+)	1463	1470	δ_dCH$_3$ (71+), ρCH$_3$ (12+)
1440	1435	νC2N3 (46−), νN1C2 (35+), δ_dCH$_3$ (20−)	1440	1428	νN1C2 (52−), νC2N3 (37+), δC2D (13−)
1390	1386	δ_sCH$_3$ (83+), νC4C6 (12+)	1390	1390	δ_sCH$_3$ (100+)
1358	1372	νC5N1 (29−), νN1C2 (24+), δN1D (17−)	1358	1359	νN3C4 (50−), νC4C5 (17+), δring1 (16+)
1296	1296	νN3C4 (43−), νC2N3 (32+), δring2 (17−)	1296	1313	νN1C2 (33+), νC2N3 (19+), νC5N1 (15−)
1250	1245	νC5N1 (34−), δC5H (25+), νC4C6 (20+)	1244	1242	δC5H (50+), νC5N1 (22−), νC4C6 (14+)
1132	1132	δC5H (31+), νN1C2 (16+), νC5N1 (13+)	1132	1143	νC5N1 (57+), δC5H (18+), δC2D (8+)
1028	1023	δring2 (16+), δring1 (13+), νC4C5 (13−)	1039	1039	δring2 (24+), δC2D (15−), νC4C6 (11+)
1004	997	ρCH$_3$ (45+), νN3C4 (21+), νC4C5 (7−)	1015	1009	ρCH$_3$ (56+), νC4C5 (15−), δC5H (6+)
953	950	δring2 (29−), δring1 (24+), δN1D (13−)	942	944	δring1 (56+), δring2 (14−), νC2N3 (6−)
	883	δC2D (23+), δN1D (19+), δring2 (18−)		894	δN3D (35+), νN3C4 (20+), δring2 (13+)
	820	δN1D (40−), δC2D (35+), δring1 (13−)		831	δC2D (46−), δN3D (27+), δring1 (15−)
	650	νC4C6 (41+), δring1 (26+), δring2 (13+)		639	νC4C6 (39+), δring2 (32−), νN3C4 (6+)
	329	δC4C6 (92−), ρCH$_3$ (13−)		314	δC4C6 (92−), ρCH$_3$ (11−)

[a] Wavenumbers (cm^{-1}) observed at 5 °C. Taken from Table 2. [b] Calculated wavenumbers in cm^{-1}. [c] Potential energy distribution (%) followed by the relative vibrational phase.

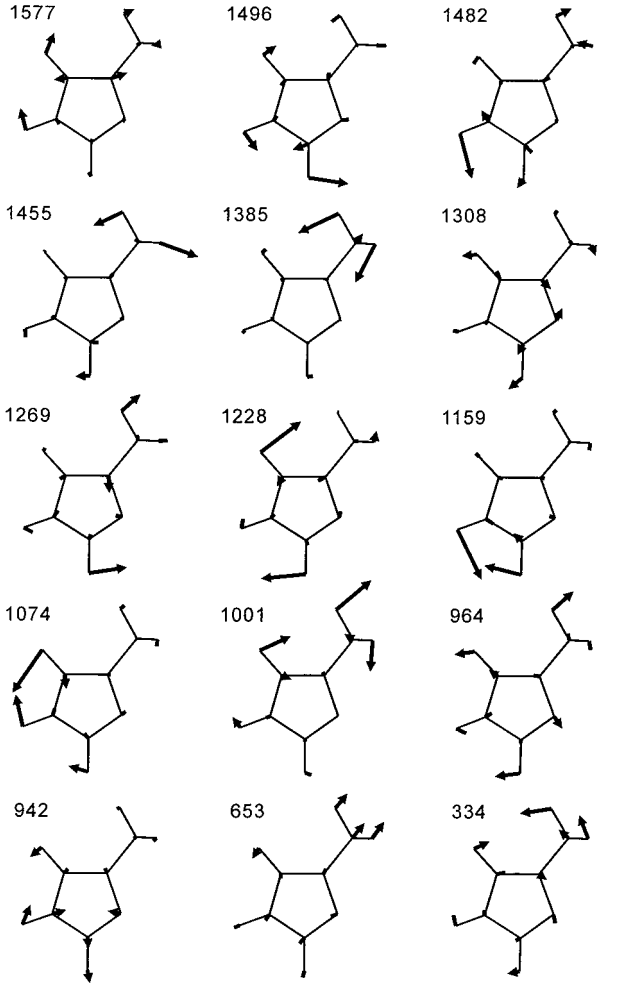

Figure 5. Normal modes calculated for the in-plane vibrations (below 1600 cm^{-1}) of the N1-H tautomer of 4-MeIm. The atomic displacement vectors are enlarged three times.

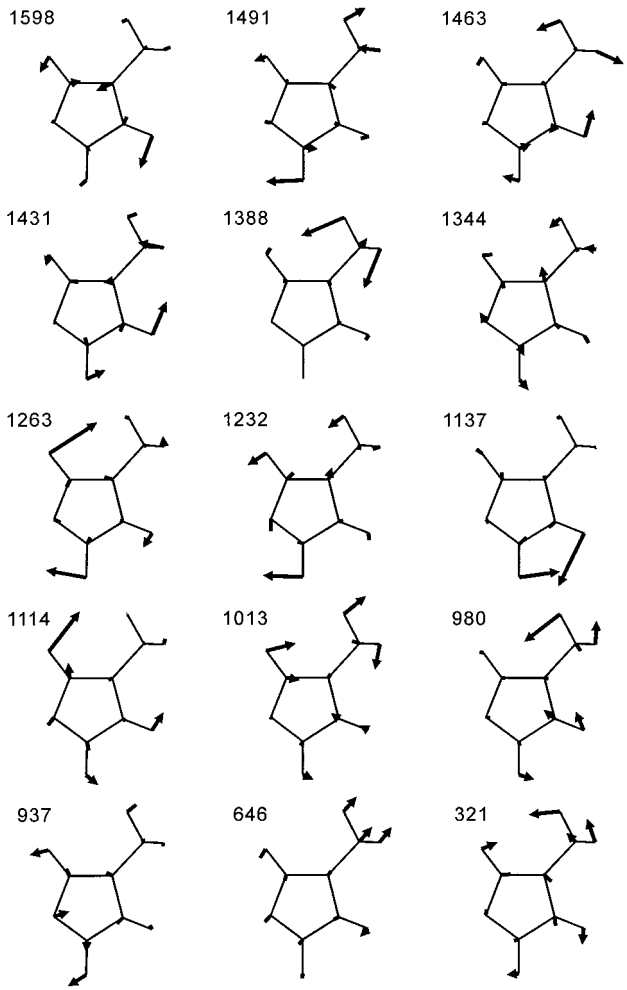

Figure 6. Normal modes calculated for the in-plane vibrations (below 1600 cm^{-1}) of the N3-H tautomer of 4-MeIm. The atomic displacement vectors are enlarged three times.

environment. Table 5 lists the scaling factors used for the diagonal elements of the force constant matrix expressed in terms of the internal symmetry coordinates. The off-diagonal elements of the force constant matrix were scaled with the geometrical means of the scaling factors for the corresponding diagonal elements.[25] These scaling factors were determined by the least-squares fitting of the calculated wavenumbers to the experimental ones. The average value of the scaling factors obtained is 0.9945. The scaling factors for the N_p-C2 (f_2, 1.0978) and N_n-C2 (f_3, 0.9212) stretches are significantly larger and smaller than the average value, respectively, indicating that partial double-bond characters of the N_p-C2 and N_n-C2 bonds increase and decrease, respectively, upon hydrogen bonding in aqueous solution. It is also noted that the hydrogen bonding increases the practical force constant for the N−H bend (f_5 for

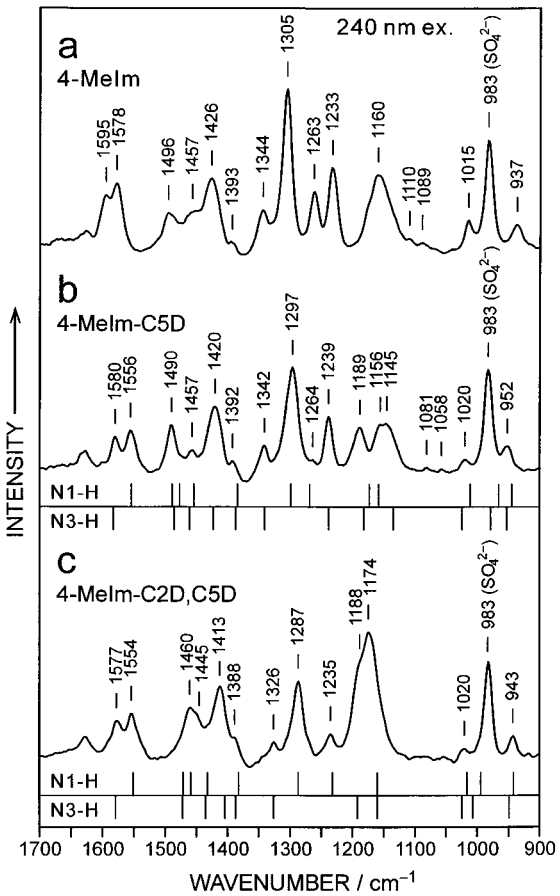

Figure 7. UV (240 nm) Raman spectra of (a) 4-MeIm, (b) 4-MeIm-C5D, and (c) 4-MeIm-C2D,C5D in H_2O solution. The sample concentration was about 50 mM. The 983 cm^{-1} band is due to SO_4^{2-} added as an internal intensity standard. The calculated wavenumbers are indicated with vertical bars extending upward (N1-H tautomer) or downward (N3-H tautomer).

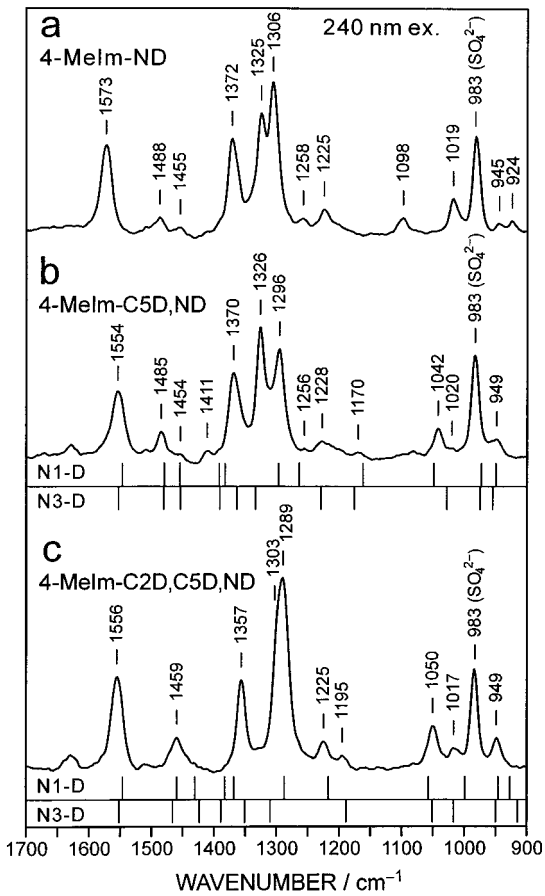

Figure 8. UV (240 nm) Raman spectra of (a) 4-MeIm, (b) 4-MeIm-C5D, and (c) 4-MeIm-C2D,C5D in D_2O solution. The sample concentration was about 50 mM. The 983 cm^{-1} band is due to SO_4^{2-} added as an internal intensity standard. The calculated wavenumbers are indicated with vertical bars extending upward (N1-H tautomer) or downward (N3-H tautomer).

δN_pH, 1.0367) at the protonated nitrogen and decreases the force constant for the ring deformation (f_7 for δring1, 0.9370) at the nonprotonated nitrogen. The calculated wavenumbers and potential energy distributions are given in Tables 6−9 for the N1-H and N3-H tautomers of 4-MeIm, 4-MeIm-C2D, 4-MeIm-ND, and 4-MeIm-C2D,ND. The root-mean-square deviation of the calculated wavenumbers from the experimental ones is 6.3 cm^{-1}. The normal modes of in-plane vibrations below 1600 cm^{-1} are depicted for 4-MeIm in Figure 5 (N1-H tautomer) and Figure 6 (N3-H tautomer).

To test the reliability of our force field, we have calculated the vibrational wavenumbers of four additional isotopomers, 4-MeIm-C5D and 4-MeIm-C2D,C5D in H_2O and D_2O solutions. The experimental wavenumbers to be compared with the calculated ones were taken from the UV (240 nm) resonance Raman spectra (Figures 7 and 8). Wavenumbers of a few vibrations that were not detected in our UV Raman spectra were taken from the paper of Bellocq et al.,[24] who reported the visible Raman and infrared spectra of 4-MeIm-C2D,C5D in H_2O and D_2O solutions. Tables 10 and 11 compare the calculated wavenumbers with the experimental ones for 4-MeIm-C5D and 4-MeIm-C2D,C5D in H_2O and D_2O solutions. The calculated band positions are indicated with vertical bars in the UV Raman spectra in Figures 7 and 8. A good agreement is seen between the calculated and observed wavenumbers (standard error, 7.0 cm^{-1}), giving support for the reliability of our force field.

Vibrational Modes of Tautomer Markers. As shown in Table 1, the N1-H and N3-H tautomers of 4-MeIm give nine pairs of tautomerism-sensitive Raman bands at 1576/1596, 1452/1427, 1304/1344, 1265/1259, 1229/1234, 1165/1149, 1088/1104, 996/1014, and 942/934 cm^{-1}. We will discuss the vibrational modes of the possible tautomer marker bands of 4-MeIm in relation to the previously proposed tautomer marker bands of histidine.

The 1576/1596 cm^{-1} bands are assigned to the C4═C5 stretch (Table 6). A significant difference between the tautomers is seen in the contribution of the N_p−H bend. In the N3-H tautomer, the C4═C5 stretch mode is definitely coupled with the N3−H bend, whereas the same mode is not significantly coupled with the N1−H bend in the N1-H tautomer. The strong coupling with the N_p−H bend in the N3-H tautomer may be related to the large atomic displacement of C4 compared to that of C5 (Figures 5 and 6), reflecting its vibrational mode like a C5═C4−C6 antisymmetric stretch (Table 6). The upshift of the C4═C5 stretch by 20 cm^{-1} in the N3-H tautomer is thus ascribed to the vibrational coupling with the N3−H bend. Actually, upon N-deuteration, the coupling diminishes and the C4═C5 stretching wavenumbers of both tautomers become closer to each other (1569 and 1576 cm^{-1}, Table 8). The 1576/1596 cm^{-1} bands of 4-MeIm correspond to the 1568/1585 cm^{-1} bands of histidine.[6] The substitution from CH_3 (4-MeIm) to CH_2 (histidine) at the C6 position seems to slightly decrease the C4═C5 stretch force constant. For both 4-MeIm and histidine, the C4═C5 stretch vibration is useful in identifying tautomers in H_2O solution but not in D_2O solution.

TABLE 10: Observed and Calculated Wavenumbers of the C5D and C2D,C5D Isotopomers of 4-MeIm in H_2O

	N1-H tautomer		N3-H tautomer	
ν_{obs} [a]	ν_{calc} [b]	assignment (PED)[c]	ν_{calc} [b]	assignment (PED)[c]
4-MeIm-C5D				
1580			1583	νC4C5 (39−), δN3H (24+), νC4C6 (16+)
1556	1554	νC4C5 (52+), νC4C6 (15−), δN1H (9+)		
1490	1489	δC2H (25+), νC2N3 (24−), δN1H (22+)	1486	δ_dCH$_3$ (28+), δC2H (27+), νN1C2 (23+)
	1477	νN1C2 (49+), δN1H (26−), δC2H (14+)		
1457	1454	δ_dCH$_3$ (75+)	1461	δ_dCH$_3$ (41+), νC2N3 (27+), δC2H (17−)
1420			1423	νC4C5 (26−), δN3H (23−), δ_dCH$_3$ (17+)
1392	1384	δ_sCH$_3$ (99−)	1387	δ_sCH$_3$ (91−)
1342			1341	νN1C2 (35+), νN3C4 (29+), δring2 (9−)
1297	1299	νC2N3 (47−), νN3C4 (33+), δring2 (14+)		
1264	1269	νN3C4 (27+), δC2H (15+), νC4C6 (14−)		
1239			1238	δC2H (31+), νN1C2 (21−), νN3C4 (12+)
1189	1173	νC5N1 (52+), δC2H (19−), δC5D (14−)	1182	νC5N1 (64+), δC5D (16−), νC2N3 (13+)
1156	1158	νN1C2 (47+), δN1H (28+), δC2H (13−)		
1145			1134	νC2N3 (35+), δN3H (30−), δC2H (14+)
1020	1011	ρCH$_3$ (43+), δring2 (23+), νC5N1 (10−)	1024	ρCH$_3$ (29+), δring2 (19−), νC4C6 (10−)
	966	νN3C4 (30+), δring2 (29−), ρCH$_3$ (19+)	979	δring2 (32+), ρCH$_3$ (29+), νN3C4 (22+)
952	945	δring1 (64+), νC4C5 (10−), νN3C4 (8−)	953	δring1 (51+), ρCH$_3$ (8+), νN3C4 (7+)
	813	δC5D (69+), δring2 (12+)	838	δC5D (65+), δring1 (15−), νC5N1 (8+)
	644	νC4C6 (39+), δring1 (26+), δring2 (11+)	640	νC4C6 (39+), δring2 (31−), νN3C4 (6+)
	328	δC4C6 (93−), ρCH$_3$ (13−)	316	δC4C6 (93+), ρCH$_3$ (11+)
4-MeIm-C2D,C5D				
1577			1579	νC4C5 (42−), δN3H (22+), νC4C6 (17+)
1554	1551	νC4C5 (55+), νC4C6 (17−), δring1 (6+)		
	1471	δN1H (51−), νN1C2 (31+), νC5N1 (12−)	1472	δ_dCH$_3$ (72+), ρCH$_3$ (13+), νN3C4 (8−)
1460	1459	δ_dCH$_3$ (67+), ρCH$_3$ (7+)		
1445	1432	νC2N3 (56−), νN1C2 (27+), δC2D (15+)	1435	νC2N3 (49+), νN1C2 (38−), δN3H (11+)
1413			1404	νN1C2 (26+), νC4C5 (21+), δN3H (19+)
1388	1382	δ_sCH$_3$ (98+)	1387	δ_sCH$_3$ (87+)
1326			1326	νN3C4 (33-), νN1C2 (20−), νC4C6 (9+)
1287	1287	νN3C4 (56−), νC2N3 (23+), δring2 (18−)		
1235	1232	νC5N1 (42−), νC4C6 (13+), νC2N3 (10−)		
1188			1192	νC5N1 (77+), νC4C6 (12−)
1174	1160	νN1C2 (30+), δN1H (27+), νC5N1 (21−)	1160	νC2N3 (40−), δN3H (27+), νN1C2 (9−)
1020	1016	ρCH$_3$ (51+), νN3C4 (10+), δring2 (9+)	1024	ρCH$_3$ (26+), δring2 (22−), νC4C6 (10−)
1000[d]	994	δring2 (22+), νN3C4 (19−), δring1 (12+)	1007	ρCH$_3$ (31−), νN3C4 (24−), δC2D (13+)
943	942	δring1 (36−), δring2 (27+), νC4C5 (9+)	949	δring1 (60+), δring2 (19−)
	884	δC2D (45+), δC5D (20+), δring1 (14−)	898	δC2D (37+), δC5D (33+), ρCH$_3$ (12+)
	795	δC5D (50+), δC2D (16−), δring2 (12+)	810	δC5D (38−), δC2D (26+), δring1 (16+)
	642	νC4C6 (39+), δring1 (26+), δring2 (10+)	639	νC4C6 (39+), δring2 (31−), νN3C4 (7+)
	326	δC4C6 (92−), ρCH$_3$ (13−)	313	δC4C6 (92−), ρCH$_3$ (11−)

[a] Observed wavenumbers in cm^{-1}. [b] Calculated wavenumbers in cm^{-1}. [c] Potential energy distribution (%) followed by the relative vibrational phase. [d] Raman wavenumbers reported by Bellocq et al.[24]

The vibrational modes of the 1452/1427 cm^{-1} bands largely differ from each other (Table 6). The 1452 cm^{-1} band of the N1-H tautomer is predominantly contributed from the degenerate deformation of the CH_3 group, whereas the 1427 cm^{-1} band of the N3-H tautomer arises from a coupled modes of the N3−H bend, CH_3 degenerate deformation, and C4═C5 stretch. The protonated nitrogen is closer to the CH_3 group in the N3-H tautomer than in the N1-H tautomer, and this proximity may cause a stronger coupling between the N_p−H bend and the CH_3 deformation in the N3-H tautomer. In histidine, however, the CH_3 group of 4-MeIm is replaced with a CH_2 group and the coupling between the N3−H (Nπ-H) bend and the CH_2 deformation may not occur. Actually, no tautomer marker bands have been found in the 1480−1400 cm^{-1} region for histidine.[6]

A common characteristics of the band pair at 1304/1344 cm^{-1} is large contributions of the N_n−C2 stretch and the N3−C4 stretch (Table 6 and Figures 5 and 6). In the 1304 cm^{-1} mode of the N1-H tautomer, the N3−C2 stretch is coupled with the N3−C4 stretch out of phase, while the N1−C2 stretch is coupled with the N3−C4 stretch in phase in the 1344 cm^{-1} mode of the N3-H tautomer. The wavenumber downshift on N-deuteration is negligible for the 1304 cm^{-1} band of the N1-H tautomer, but it amounts to 21 cm^{-1} for the 1344 cm^{-1} band of the N3-H tautomer (1304/1323 cm^{-1}, Figure 3b and Table 8). Despite the large downshift of the N3-H tautomer marker, the wavenumber difference between the marker bands still remains about 20 cm^{-1}. In the visible and UV Raman spectra of 4-MeIm in D_2O solution, the 1304/1323 cm^{-1} bands are well resolved (Figures 3b and 8a), indicating the utility of the bands as tautomer markers in D_2O solution as well as in H_2O solution. A pair of Raman bands is seen at 1320/1354 cm^{-1} for histidine,[6] and it is likely to be the counterpart of the 1304/1344 cm^{-1} pair of 4-MeIm. The wavenumber difference between 4-MeIm and histidine may be ascribed to a small increase of the N3−C4 stretch force constant induced by the CH_3 (4-MeIm) → CH_2 (histidine) substitution at C6 through the C4−C6 linkage. In the Raman spectra reported previously,[6] the relative intensity of the 1320/1354 cm^{-1} Raman bands seems to change with temperature, though the temperature dependence was not explicitly stated in the paper.[6] We propose that the 1320/1354 cm^{-1} bands are new tautomer markers of histidine. Since UV excitation enhances the Raman bands of histidine in the 1350−1320 cm^{-1} region,[9] the 1320/1354 cm^{-1} bands may be useful in analyzing the tautomeric state of histidine by UV Raman spectroscopy.

Exchange of vibrational mode occurs between the band pairs at 1265/1259 and 1229/1234 cm^{-1} on going from the N1-H to N3-H tautomer (Table 6). In the N1-H tautomer, the 1265 cm^{-1} band arises mainly from the N3(N_n)−C4 stretch and the 1229 cm^{-1} band from the C5−H bend. In the N3-H tautomer, on the contrary, the 1259 cm^{-1} band is contributed mainly from the C5−H bend and the 1234 cm^{-1} band from the N1(N_n)−C5 stretch. Accordingly, the correct pairing of the tautomer marker bands in this wavenumber region may be described as 1265/1234 (N_n−C4/C5 stretch) and 1229/1259 cm^{-1} (C5−H bend). In the 1300−1200 cm^{-1} region of the Raman spectrum of histidine, three bands are seen at 1282, 1260, and 1230 cm^{-1}, of which the former two bands are assigned to the Nτ-H (N1-H) and Nπ-H (N3-H) tautomers, respectively.[6] The 1282 cm^{-1} band of histidine is correlated with the 1265 cm^{-1} band of

TABLE 11: Observed and Calculated Wavenumbers of the C5D and C2D,C5D Isotopomers of 4-MeIm in D_2O

	N1-D tautomer		N3-D tautomer	
ν_{obs} [a]	ν_{calc} [b]	assignment (PED)[c]	ν_{calc} [b]	assignment (PED)[c]
4-MeIm-C5D,ND				
1554	1547	νC4C5 (57−), νC4C6 (19+), δring1 (8−)	1553	νC4C5 (55−), νC4C6 (20+), δring2 (6+)
1485	1480	δC2H (39+), νC2N3 (34−), νN1C2 (20+)	1481	δC2H (30+), νN1C2 (28+), δ_dCH$_3$ (26+)
1454	1455	δ_dCH$_3$ (78+), νC2N3 (8+)	1454	δ_dCH$_3$ (56−), νN1C2 (16+), δC2H (15+)
1411	1392	νN1C2 (52−), δN1D (19+), νC5N1 (16+)		
	1383	δ_sCH$_3$ (91+)	1391	δ_sCH$_3$ (97+)
1370			1364	νC2N3 (36+), νN3C4 (35−), νC4C5 (18+)
1326			1334	νN1C2 (38+), νN3C4 (15+), δring2 (11−)
1296	1297	νC2N3 (41−), νN3C4 (40+), δring2 (16+)		
1256	1264	δC2H (21+), νN3C4 (20+), νC4C6 (13−)		
1228			1230	δC2H (33−), νN1C2 (15+), νC5N1 (11−)
1170	1162	νC5N1 (43+), δC2H (26−), δC5D (14−)	1176	νC5N1 (70−), δC5D (16+), δC2H (12+)
1042	1049	ρCH$_3$ (26+), δring2 (16+), νN1C2 (12−)		
1020			1028	ρCH$_3$ (36−), δring1 (11+), δring2 (8+)
	973	ρCH$_3$ (36+), νN3C4 (34+), δring1 (15−)	975	δring2 (37+), νN3C4 (13+), νC2N3 (11+)
949	950	δring2 (38+), δring1 (28−), νC4C5 (4+)	955	δring1 (38+), ρCH$_3$ (17+), νN3C4 (13+)
	869	δN1D (48+), δring1 (16+), δC5D (10+)	885	δN3D (62+), δring1 (19−), ρCH$_3$ (6+)
	793	δC5D (56+), δN1D (16−), νC5N1 (11+)	834	δC5D (60+), δring1 (10−), νC5N1 (7+)
	643	νC4C6 (38+), δring1 (26+), δring2 (11+)	633	νC4C6 (37+), δring2 (30−), νN3C4 (7+)
	326	δC4C6 (92+), ρCH$_3$ (13+)	311	δC4C6 (92−), ρCH$_3$ (11−)
4-MeIm-C2D,C5D,ND				
1556	1546	νC4C5 (58+), νC4C6 (20−), δring1 (9+)	1552	νC4C5 (57−), νC4C6 (21+), δring2 (7+)
1459	1459	δ_dCH3 (75+), ρCH$_3$ (8+)	1466	δ_dCH$_3$ (76+), ρCH$_3$ (11+)
1439[d]	1430	νC2N3 (53+), νN1C2 (39−), δC2D (14−)	1423	νN1C2 (59−), νC2N3 (41+), δC2D (14−)
1389[d]	1383	δ_sCH$_3$ (91+)	1389	δ_sCH$_3$ (99+)
1357	1368	νN1C2 (29+), νC5N1 (27−), δN1D (20−)	1351	νN3C4 (51+), νC4C5 (19−), δring1 (15−)
1303			1310	νN1C2 (27−), νC2N3 (22−), νC5N1 (12+)
1289	1287	νN3C4 (56+), νC2N3 (23−), δring2 (18+)		
1225	1217	νC5N1 (52−), νC4C6 (14+), δC5D (8+)		
1195			1189	νC5N1 (78−), νC4C6 (11+), δC5D (10+)
1050	1057	ρCH$_3$ (36+), δN1D (11−), δring2 (10+)	1051	ρCH$_3$ (38+), δC2D (20−), δN3D (11−)
1017	999	νN3C4 (30+), δring1 (17−), δC2D (13−)	1017	δring2 (27+), νC4C6 (13+), δring1 (10+)
949	946	δring2 (34+), δring1 (20−), δN1D (11+)	950	δring1 (44+), δring2 (8−), ρCH$_3$ (6+)
918[d]	927	ρCH$_3$ (19−), δC2D (18−), δC5D (13−)	915	ρCH$_3$ (22+), δC2D (19+), δC5D (16+)
	819	δN1D (44−), δC2D (30+), δring1 (14−)	852	δN3D (42−), δC5D (18+), δC2D (11+)
	788	δC5D (55+), δring2 (13+), νC5N1 (10+)	807	δC5D (32+), δC2D (30−), δring1 (16−)
	641	νC4C6 (38+), δring1 (26+), δring2 (11+)	632	νC4C6 (37+), δring2 (31−), νN3C4 (7+)
	324	δC4C6 (92+), ρCH$_3$ (13+)	309	δC4C6 (92−), ρCH$_3$ (11−)

[a] Observed wavenumbers in cm^{-1}. [b] Calculated wavenumbers in cm^{-1}. [c] Potential energy distribution (%) followed by the relative vibrational phase. [d] Raman wavenumbers reported by Bellocq et al.[24]

4-MeIm. Since the 1265 cm^{-1} band has a significant contribution from the N3−C4 stretch (Table 6), the large wavenumber upshift on going from 4-MeIm to histidine may also be ascribed to the increase of the N3−C4 stretch force constant, which was assumed above to explain similar upshifts of the 1304/1344 cm^{-1} bands. The remaining 1260 cm^{-1} band of histidine is assigned to the C5−H bend of the Nπ-H (N3-H) tautomer (1259 cm^{-1}) and the 1230 cm^{-1} band to an overlap of the N1−C5 stretch of the Nπ-H (N3-H) tautomer (1234 cm^{-1}) and the C5−H bend of the Nτ-H (N1-H) tautomer (1229 cm^{-1}). In D_2O solution, the tautomer marker Raman bands of histidine have been observed at 1278 and 1261 cm^{-1},[26] which correspond to the 1258/1223 and 1223/1251 cm^{-1} bands of 4-MeIm-ND (Table 8).

Overlapping of two broad bands at 1165 (N1-H tautomer) and 1149 cm^{-1} (N3-H tautomer) produces a very broad band around 1155 cm^{-1} in the Raman spectrum of 4-MeIm in H_2O solution (see Figure 2b and Table 1). These bands have significant contributions from the N_p−C2 stretch and the N_p−H bend (Table 6). Owing to their vibrational modes localized at the protonated nitrogen, the wavenumbers of these bands are expected to be sensitive to the hydrogen bond at the protonated nitrogen. Actually, the band of the N1-H tautomer has been reported to shift to 1191 cm^{-1} in the solid state.[17] These bands may be useful as markers not only of tautomerism but also of hydrogen bonding at the protonated nitrogen. In the Raman spectrum of histidine in H_2O solution, a broad band is seen at 1159 cm^{-1}.[6]

Both bands of the 1088/1104 cm^{-1} pair are assigned to the C5−N1 stretch coupled with the C5−H bend (Table 6). A small contribution of the N1−H bend is also seen for the N1-H tautomer (Table 6). The coupling with the N1−H bend may be the origin of the wavenumber downshift in the N1-H tautomer compared to the N3-H tautomer. Upon N-deuteration, the 1088 cm^{-1} band of the N1-H tautomer shifts up to 1095 cm^{-1} and overlaps the practically unshifted 1102 cm^{-1} band of the N3-H tautomer (Figure 3b and Table 8). Since the overlap of the bands is extensive in D_2O solution, the C5−N1 stretch vibration may be useful only in H_2O solution. Noguchi et al. demonstrated the utility of the C5−N1 stretch bands of histidine at ∼1090/1105 cm^{-1} as tautomer markers in infrared spectra.[12]

The 996/1014 cm^{-1} bands are significantly contributed from the CH_3 rocking (Table 6). Other contributors are the C4−C5 stretch and the ring deformation at the protonated nitrogen (δring2). The contribution of the CH_3 rocking is especially large for the 996 cm^{-1} band of the N1−H tautomer. In the UV resonance Raman spectrum of 4-MeIm excited at 218 nm, no band is seen around 996 cm^{-1}.[9] This observation is consistent with the large contribution of the CH_3 rocking to the 996 cm^{-1} vibration because vibrations of a CH_3 group would not be enhanced by UV excitation. Ashikawa and Itoh found tautomer marker Raman bands at 983 (Nτ-H) and 1004 cm^{-1} (Nπ-H) for histidine and correlated them with the 996 (N1-H) and 1014 cm^{-1} (N3-H) bands of 4-MeIm.[6] However, the 983 cm^{-1} band of histidine is unlikely to have the same origin as that of the 996 cm^{-1} band of 4-MeIm because the 983 cm^{-1} band is enhanced with 218 nm excitation in contrast to no enhancement of the 996 cm^{-1} band.[9] A possible origin of the 983 cm^{-1} band is the N3−C4 stretching mode coupled with δring2, which is observed at 977 cm^{-1} in the visible Raman spectrum of 4-MeIm (Figure 2b and Table 6) and enhanced with 218 nm excitation.[9] Since the 977 cm^{-1} band has a significant contribution of the N3−C4 stretch as the 1265 cm^{-1} band discussed above, the $CH_3 \rightarrow CH_2$ substitution may raise the wavenumber of this mode

specifically for the Nτ-H (N1-H) tautomer in a mechanism similar to that proposed for the 1265 cm^{-1} band.

Both of the 934/942 cm^{-1} bands are assigned to the ring deformation at the nonprotonated nitrogen (δring1, see Table 6). Because of the small wavenumber separation, they are severely overlapped with each other and may not be useful as a marker of tautomerism. The δring1 mode is expected to be sensitive to the hydrogen bonding at the nonprotonated nitrogen, and it gives a prominent band in UV Raman spectra (Figure 9a and ref 9). Accordingly, the δring1 band may be useful as a marker of hydrogen bonding or metal coordination at the nonprotonated nitrogen. It has been reported that 4-MeIm gives a single band at 926 cm^{-1} in the solid state[17] and Cu(II)-coordinated imidazole produces a strong UV resonance Raman band at 954 cm^{-1}.[9]

Conclusion

We have examined in-plane vibrations of 4-MeIm by Raman spectroscopy and DFT calculations. Nine pairs of Raman bands at 1576/1596, 1452/1427, 1304/1344, 1265/1259, 1229/1234, 1165/1149, 1088/1104, 996/1014, and 942/934 cm^{-1} are identified as possible markers of the N1-H/N3-H tautomers. The force constants calculated by the DFT method and scaled with nine scaling factors are successful to reproduce the Raman wavenumbers observed for the N1-H and N3-H tautomers of 4-MeIm and its seven isotopomers. Among the possible tautomer markers, two pairs of bands at 1165/1149 and 942/934 cm^{-1} are expected to be more sensitive to hydrogen bonding and/or metal coordination. Three pairs of bands at 1576/1596 (C4═C5 stretch), 1304/1344 (N_n−C2 stretch), and 1088/1104 cm^{-1} (C5−N1 stretch) are useful as tautomer markers of 4-MeIm. The corresponding bands of histidine are located at 1568/1585, 1320/1354, and 1090/1105 cm^{-1}. In addition to the known tautomer markers at 1568/1585 and 1090/1105 cm^{-1},[6] the 1320/1354 cm^{-1} bands are proposed to be new tautomer markers of histidine. The vibrational modes of the other tautomer marker bands of histidine are suggested to be the N3−C4 stretch (1282 cm^{-1}) and the N3−C4 stretch + δring2 (983 cm^{-1}) for the Nτ-H tautomer and the C5−H bend (1260 cm^{-1}) and δring2 (1004 cm^{-1}) for the Nπ-H tautomer. It is also noted that the differences in tautomer marker wavenumber between 4-MeIm and histidine are consistently explained by assuming a decrease of the C4═C5 stretch force constant and an increase of the N3−C4 stretch force constant associated with the CH_3 (4-MeIm) → CH_2 (histidine) substitution at C6. The detailed vibrational modes revealed here may be useful in analyzing the Raman and infrared spectra of histidine residues in proteins.

References and Notes

(1) Reynolds, W. F.; Peat, I. R.; Freeman, M. H.; Jyerla, J. R., Jr. *J. Am. Chem. Soc.* **1973**, *95*, 328.

(2) Blomberg, F.; Maurer, W.; Rüterjans, H. *J. Am. Chem. Soc.* **1977**, *99*, 8149.

(3) Ash, E. L.; Sudmeier, J. L.; De Fabo, E. C.; Bachovchin, W. W. *Science* **1997**, *278*, 1128.

(4) Schultz, L. W.; Quirk, D. J.; Raines, R. T. *Biochemistry* **1998**, *37*, 8886.

(5) Okar, D. A.; Live, D. H.; Kirby, T. L.; Karschnia, E. J.; von Weymarn, L. B.; Armitage, I. M.; Lange, A. J. *Biochemistry* **1999**, *38*, 4471.

(6) Ashikawa, I.; Itoh, K. *Biopolymers* **1979**, *18*, 1859.

(7) Tasumi, M.; Harada, I.; Takamatsu, T.; Takahashi, S. *J. Raman Spectrosc.* **1982**, *12*, 149.

(8) Chinsky, L.; Jolles, B.; Laigle, A.; Turpin, P. Y. *J. Raman Spectrosc.* **1985**, *16*, 235.

(9) Caswell, D. S.; Spiro, T. G. *J. Am. Chem. Soc.* **1986**, *108*, 6470.

(10) Takeuchi, H.; Kimura, Y.; Koitabashi, I.; Harada, I. *J. Raman Spectrosc.* **1991**, *22*, 233.

(11) Hashimoto, S.; Takeuchi, H. *J. Am. Chem. Soc.* **1998**, *120*, 11012.

(12) Noguchi, T.; Inoue, Y.; Tang, X.-S. *Biochemistry* **1999**, *38*, 10187.

(13) Majoube, M.; Millié, Ph.; Vergoten, G. *J. Mol. Struct.* **1995**, *344*, 21.

(14) Gallouj, H.; Lagant, P.; Vergoten, G. *J. Raman Spectrosc.* **1997**, *28*, 909.

(15) Stephens J. P.; Devlin, F. J.; Chabalowski, C. F.; Frisch M. J. *J. Phys. Chem.* **1994**, *98*, 11623.

(16) Becke, A. D. *J. Chem. Phys.* **1993**, *98*, 5648.

(17) Hasegawa, K.; Ono, T.; Noguchi, T. *J. Phys. Chem. B* **2000**, *104*, 4253.

(18) Hashimoto, S.; Ono, K.; Takeuchi, H.; Harada, I. *Spectrochim. Acta* **1994**, *50A*, 1647.

(19) Thompson, W. J. *Comput. Phys.* **1993**, *7*, 627.

(20) Takeuchi, H.; Harada, I. *J. Raman Spectrosc.* **1990**, *21*, 509.

(21) Frisch, M. J.; Trucks, G. W.; Schlegel, H. B.; Scuseria, G. E.; Robb, M. A.; Cheeseman, J. R.; Zakrzewski, V. G.; Montgomery, J. A., Jr.; Stratmann, R. E.; Burant, J. C.; Dapprich, S.; Millam, J. M.; Daniels, A. D.; Kudin, K. N.; Strain, M. C.; Farkas, O.; Tomasi, J.; Barone, V.; Cossi, M.; Cammi, R.; Mennucci, B.; Pomelli, C.; Adamo, C.; Clifford, S.; Ochterski, J.; Petersson, G. A.; Ayala, P. Y.; Cui, Q.; Morokuma, K.; Malick, D. K.; Rabuck, A. D.; Raghavachari, K.; Foresman, J. B.; Cioslowski, J.; Ortiz, J. V.; Baboul, A. G.; Stefanov, B. B.; Liu, G.; Liashenko, A.; Piskorz, P.; Komaromi, I.; Gomperts, R.; Martin, R. L.; Fox, D. J.; Keith, T.; Al-Laham, M. A.; Peng, C. Y.; Nanayakkara, A.; Challacombe, M.; Gill, P. M. W.; Johnson, B.; Chen, W.; Wong, M. W.; Andres, J. L.; Gonzalez, C.; Head-Gordon, M.; Replogle, E. S.; Pople, J. A. *Gaussian 98*, Revision A.9; Gaussian, Inc.; Pittsburgh, PA, 1998.

(22) Shimanouchi, T. *Computer Programs of Normal Coordinate Treatment of Polyatomic Molecules*; The University of Tokyo: Tokyo, 1968.

(23) Shimanouchi, T.; Matsuura, H.; Ogawa, Y.; Harada, I. *J. Phys. Chem. Ref. Data* **1978**, *7*, 1323.

(24) Bellocq, A.-M.; Garrigou-Lagrange, C. *J. Chim. Phys.* **1969**, *66*, 1511.

(25) Pulay, P.; Fogarasi, G. *J. Chem. Phys.* **1981**, *74*, 3999.

(26) Miura, T.; Satoh, T.; Hori-i, A.; Takeuchi, H. *J. Raman Spectrosc.* **1998**, *29*, 41.